



Structural change monitoring of a cable-stayed bridge by time-series modeling of the global thermal deformation acquired by GPS

Hien Van Le¹ · Mayuko Nishio²

Received: 15 March 2019 / Accepted: 9 October 2019 / Published online: 23 October 2019
© Springer-Verlag GmbH Germany, part of Springer Nature 2019

Abstract

In this study, the use of ARIMA model coefficients extracted from the response of global thermal deformation, which can be acquired by the GPS monitoring, was proposed for the structural change monitoring of the long-span bridge. The daily periodic air temperature change causes the characteristic global thermal deformation, which is suitable to be acquired by the GPS in the long-span cable-stayed bridge. The pattern of this global thermal deformation was then expected to have sensitivities to changes on global structural properties. The procedures of feature extraction based on the ARIMA model estimation and the Mahalanobis distance comparison were presented, and their applicabilities were verified both by the numerical study and by the application to actual GPS monitoring data. In the numerical study, a FE model of a cable-stayed bridge was constructed, and the time-series displacements under the periodic temperature load were obtained with some cases of structural conditions by varying the boundary conditions and the cable tensions. The procedures of feature extraction and comparison were then applied to the obtained displacement time-series. In the results, the Mahalanobis distance of feature vector, which was configured by estimated AR and MA coefficients, showed significant changes both in the two cases of boundary condition and stayed-cable tension changes. The procedure was then applied to year-round GPS data acquired in the actual cable-stayed bridge. It was shown that the Mahalanobis distance comparison could provide proper assessment to the structural changes that was consistent with the actual structural condition.

Keywords Global positioning system · Global thermal deformation · Cable-stayed bridge · ARIMA model · Mahalanobis distance

1 Introduction

The actual bridges under operations always show various static and dynamic responses due to both operational and environmental effects. In many previous studies of the structural health monitoring, those effects were analyzed in detail, e.g., [1] and [2]. In those studies, it was well understood that the most significant environmental effect on structural

responses was the air temperature change. The dynamic properties, such as resonant frequencies and the static displacement and strain, show high correlations with daily and seasonal trends of the air temperature data. The idea of this study is to use this air temperature effect as the input load to the structure in SHM. The global thermal deformation due to air temperature change is expected to show sensitivities to global structural changes, such as changes in boundary conditions of the structure. For instance, the bridge bearings, which are the movable members to determine the boundary condition, often show their property changes due to corruptions, fatigue, seismic loading histories, and so on. There is a previous study [3] that indicated that the properties of bearings greatly affected the global bending deformation of the bridge.

Considering observations of the global deformation of structures, the Global Positioning System (GPS) is becoming a common technology. The Real-Time Kinematic (RTK) technique has been successfully applied to measure

✉ Mayuko Nishio
nishio@kz.tsukuba.ac.jp

Hien Van Le
hienlv84.uct@gmail.com

¹ Faculty of Civil Engineering, University of Transport and Communications, 3 Cau Giay Street, Dong Da District, Hanoi, Vietnam

² Department of Engineering Mechanics and Energy, University of Tsukuba, 1-1-1 Tennodai, Tsukuba 305-8573, Japan

the displacements of oscillating flexible civil engineering structures such as long-span bridges and high-rise buildings, etc. There are some advantages in GPS technology to monitor the displacements of large-scale structures, such as overcoming the limitations of weather, observing the global displacements in three-dimensions with high accuracy. In addition, the GPS is improving in reducing weight and size of devices as well as providing the automatic operation. The applications of GPS to the structural monitoring of long-span bridges were mentioned in some previous studies. For instance, the global responses of a suspension bridge in earthquake and typhoon events were determined by analyzing GPS monitoring data [4]. The applicability of GPS to measure the displacement of a tall building during under extreme loadings such as earthquake and strong winds was also verified [5]. The data-processing procedure was also shown for accurate bridge displacement sensing using a GPS monitoring system [6].

The authors also worked on the study of GPS monitoring in an actual cable-stayed bridge [7]. There, a dominant deformation mode, which was the periodic in-plane global deformation due to variations in daily air temperature changes, was recognized by the correlation and frequency analysis of 4-month-long GPS displacement data acquired at the two towers and girder. In addition, the application of Autoregressive Integrated Moving Average (ARIMA) model estimation to the GPS data was also shown in expectation of using model coefficients as the feature for comparing the global thermal deformation. There are actually many previous studies that applied time-series modeling, such as AR, ARMA, and ARIMA models, to the structural monitoring data. In some studies, the time-series modeling was applied to realize the structural damage detection and classification using the structural vibration data, such as in [8]. There, the time-series modeling was applied based on the assumption of stochastic process to the structural vibration. In a recent study, the ARMA modeling was applied to GPS monitoring data to detect significant structural dynamic property changes [9]. On the other hand, some previous studies adopt the time-series modeling for the structural condition assessment from the long-term time-series data of any structural response considering the environmental and operational effects. One of those studies [10] applied the ARIMA model estimation to the time-series strain data continuously acquired during the bridge construction, and it was shown that the estimated model coefficient could be used as the features to detect structural changes in unusual events. Another recent study [11] showed the effectiveness of using the residual process, which was derived by time-series decomposition considering the heteroscedasticity of the data, for the structural change detection from the time-series SHM data. However, most of those studies do not show the application of time-series modeling to the structural change monitoring by considering

the specific input load and time-series response in the actual bridge under operation.

The idea of this study is the use of a 1-day-long time-series governed by the global deformation mode for the structural change monitoring. The daily temperature change, which has been regarded as one of the environmental effects that should be removed in the analysis of SHM data, is treated as a load that gives the response for pattern recognition. The ARIMA model coefficients are used as the comparative feature for continuously assessing the changes in the global thermal deformation due to structural changes. The global deformation, which is the response to air temperature load, is expected to show sensitivities to condition changes that are relatively global structural changes in the cable-stayed bridge, such as changes of boundary conditions and tensions of stayed-cables. The pattern of multi-point time-series displacements, which can be acquired by GPS monitoring, is evaluated by statistical measures. This paper shows the feature extraction and comparison procedure based on the ARIMA model estimation to assess those structural changes. Both a numerical study and an application to actual SHM data were conducted to show the effectiveness of idea. First, the global thermal deformation of the cable-stayed bridge, which was recognized by the analysis of GPS data in our previous study [7] is explained. The feature extraction procedure based on the ARIMA model estimation is then presented, and it is applied to the year-round time-series GPS data. A numerical study is then conducted using a finite element (FE) model of a cable-stayed bridge to verify the sensitivities of ARIMA model coefficient features to the purpose structural changes. The feature comparison procedure based on the Mahalanobis distance measure is then considered both in the numerical study and in the application to the GPS monitoring data.

2 Global thermal deformation of the cable-stayed bridge

Here, we first review our previous study [7] to show specifications of the target cable-stayed bridge and the GPS monitoring. The global thermal deformation mode, which is the response to be used for the structural change monitoring in this study, is also explained.

2.1 Target bridge and GPS monitoring

The target actual bridge is the Can Tho bridge, a long-span cable-stayed bridge located in southern Vietnam opened in 2010. The total length of the bridge is 1010 m with the center span of 550 m, the width of the box-girder is 26 m, and the heights of two towers except footings are both 165 m. The elastic rubber bearings, which allow the displacement in

the longitudinal direction, are placed at the location of link mechanism of each tower and both ends of the girder.

The SHM system was installed in 2010, consisting of several types of sensors, including GPS and temperature sensors. The GPS was installed to observe the global displacements of the bridge. The system was configured with nine rover stations and two base stations using Leica GMX 902 GG receivers. The two of nine rover stations are located on the tops of two towers, and the other seven are placed on the girders, including the upstream and downstream sides of the center and quarter spans, as shown in Fig. 1. The GPS Real-Time Kinematic (RTK) technique was adopted for measurement with specified accuracies of $\pm 10 \text{ mm} \pm 1 \text{ ppm}$ for the horizontal plane and $\pm 20 \text{ mm} \pm 1 \text{ ppm}$ for the vertical direction. The three-dimensional displacement data were sampled at 20 Hz and averaged every 10 min. Figure 2a–c shows the time-series displacement data at the center span acquired from February 15–22, 2013. The air temperature data in the same period at the center span are also shown in Fig. 2d. In Fig. 2c, which is the data in the vertical direction, the time-series displacement is clearly anticorrelated with the daily variations in air temperature; on the other hand, the data in

the longitudinal and lateral directions, which are shown in Fig. 2a, b, do not show clear correlations to the temperature. The correlation with daily temperature changes was not found in the data for all sensor locations and directions.

2.2 Global thermal deformation due to daily temperature changes

In our previous study [7], the clear correlation with daily temperature changes was found in the data of specific positions and directions. Moreover, it was also shown that the most significant frequency component of those data was the period of 24 h, i.e., component of daily temperature variations. Actually, the year-round GPS data did not clearly show the seasonal trend. This is because, in the area where the target bridge is located, Can Tho in Vietnam, the average daily temperatures do not change a lot through a year. Therefore, the dominant thermal deformation was due to the daily temperature change with the period of 24 h.

It was then found that there were five particular locations and directions of year-round GPS data that showed high correlations with daily periodic temperature changes: the data

Fig. 1 GPS sensor locations at the cable-stayed bridge

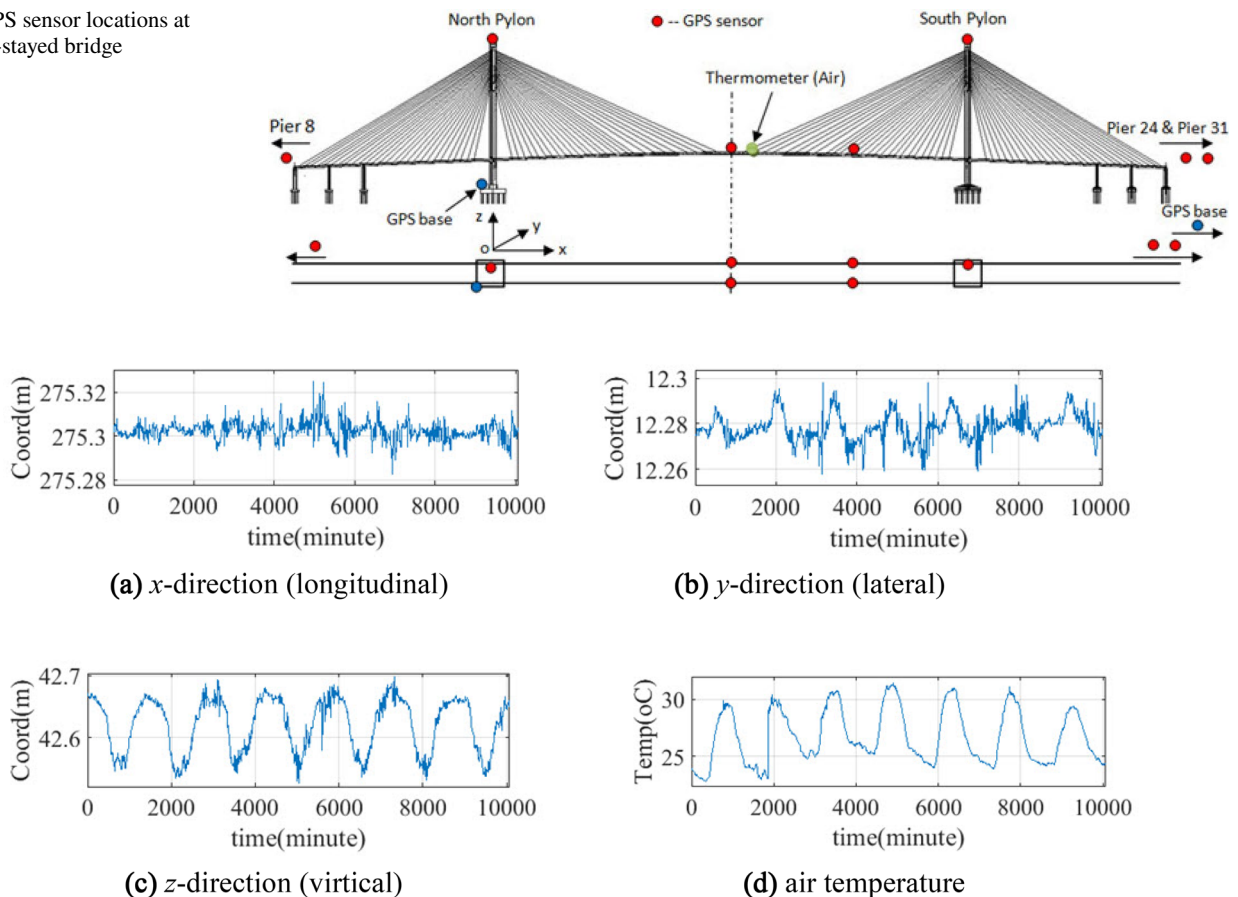


Fig. 2 1-week GPS data and air temperature at the center span (from Feb 15 to 22, 2013)

of longitudinal direction at the top of each of the north and south towers, the data of vertical direction at the center span, and the data of vertical and longitudinal directions at the quarter span. Figure 3 shows the global deformation mode, which was captured by considering whether the correlation to the temperature data was positive or negative in each of five time-series. Since the cable-stayed bridge is the large-scaled and flexible structure, the fluctuation ranges of daily periodic responses in those five time-series were around 0.1 m, as also shown in Fig. 2c. The recognized thermal deformation mode, the global in-plane deformation of the cable-stayed bridge, was not expected to show sensitivities to local damages in structural members. However, it was expected to be sensitive to global structural changes, such as changes in boundary conditions or stay-cable tensions.

3 Feature extraction by ARIMA model estimation to GPS data

The five GPS displacement data, which significantly contributed to the global deformation mode of the cable-stayed bridge, were all non-stationary time-series because they are dominated by the daily periodic trend due to air temperature changes. In our previous study [7], it was shown that the Autoregressive Integrated Moving Average (ARIMA) model was applicable to modeling those time-series displacements of the global deformation mode. There, the ARIMA model was estimated for 4-month-long GPS data acquired in the target cable-stayed bridge, and the applicability of estimated coefficients was discussed as the feature to compare the global deformation mode. In this chapter, the feature extraction procedure based on the ARIMA model estimation is presented, and the extracted features, i.e., estimated model coefficients, are shown by applying the procedure to the year-round GPS data.

3.1 Procedure of feature extraction

The Autoregressive Integrated Moving Average (ARIMA) model is often applied to time-series that show evidence for the non-stationarity [12]. It is generally defined by its orders that are called autoregressive (AR) terms with order

p , differencing order d , and moving average (MA) term with order q , respectively. The ARIMA model with p , d , and q -th orders, which is represented by $ARIMA(p, d, q)$, is then described as:

$$(1 - \varphi_1 B - \varphi_2 B^2 - \dots - \varphi_p B^p)(1 - B)^d y_t = (1 - \theta_1 B - \theta_2 B^2 - \dots - \theta_q B^q) \varepsilon_t, \tag{1}$$

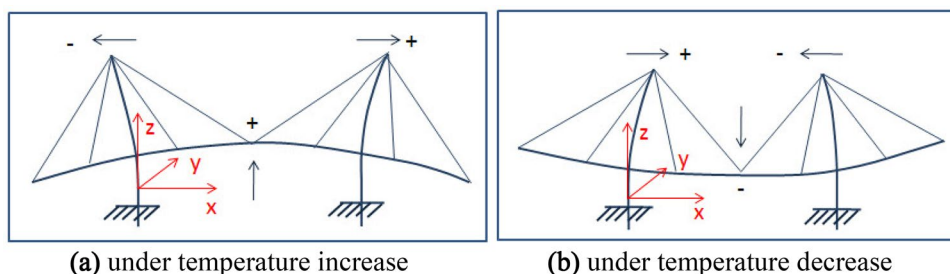
where y_t is t -th component of time-series process y , φ_i ($i = 1 - p$) and θ_j ($j = 1 - q$) are coefficients of the autoregressive (AR) terms and the moving average (MA) terms, respectively, B is the lag-operator, and ε_t is a white noise error term. The orders p , d , and q are defined to satisfy the given time-series process. Here, the original non-stationary process is transferred to a stationary process by taking differencing order d , and the orders of AR and MA terms, p and q , are determined by taking the autocorrelation function (ACF) and the partial autocorrelation function (PACF), and also using any kind of information criterion, such as the Akaike’s Information Criterion (AIC) or the Bayesian Information Criterion (BIC).

To compare the global deformation with the period of 24 h, the 24-h-long (1-day-long) time-series data should be compared day-by-day. Each 1-day-long time-series is the non-stationary process because it includes trends due to daily variation of air temperature. The feature extraction procedure based on the ARIMA model estimation was then configured as below.

Step 1 First, divide the GPS data into 1-day-long data (24-h-long data), and check the time-series process, stationary or non-stationary, by taking the ACF and PACF. The Augmented Dickey–Fuller (ADF) test is also employed to confirm a stationary or non-stationary process. In addition, the existence of data missing, which is due to some error in GPS measurement, in each time-series is also checked. When the missing data are less than two points or less, the interpolation is applied [7]. Otherwise, the time-series is removed from the dataset to be analyzed.

Step 2 Most of 1-day-long GPS data show the non-stationary process due to the 1-day trend of air temperature. The transform operation, from non-stationary to stationary, is taken by differencing the time-series with the order

Fig. 3 Global thermal deformation mode captured by GPS data



of d in ARIMA(p, d, q). Here, the daily trend can be considered of the order of $d = 1$ because there are no periodic trend components in the 1-day-long data.

Step 3 Determine the AR term order p and the MA term order q by taking the ACF and PACF functions to the differenced time-series in Step 2. In addition, the BIC is also checked for confirmation.

Step 4 AR and MA coefficients are estimated by the maximum likelihood method. Here, the Matlab function “arima” in the Box–Jenkins Model was adopted in this study.

Step 5 The ARIMA model coefficients are accepted as the feature only when the residual error of the estimated model shows the white noise process. The Ljung–Box test is conducted in this step.

The accepted AR coefficients ϕ_i ($i = 1 - p$) and MA coefficients θ_j ($j = 1 - q$) are considered the model coefficients of a properly estimated ARIMA (p, d, q) model and describe characteristics of the time-series; therefore, they can be used as the features to monitor the pattern change of the global thermal deformation.

3.2 AR and MA coefficients extracted from GPS data

The feature extraction procedure was then applied to the GPS displacements acquired from Jan 1 to Nov 30, 2013 in the target cable-stayed bridge. In most of 1-day-long data, the model orders were determined to $d = 1$, $p = 1$, and $q = 1$; therefore, the AR and MA coefficients of ARIMA(1,1,1) were adopted as the standardized comparative feature. This was because the 1-day-long time-series was the simple time-series, and the same model can be used for the comparison. In case the estimated model was not accepted in the Ljung–Box test in Step 5 because the ARIMA(1,1,1) was not proper, the coefficients were not adopted as the feature. It was recognized that the data that were not accepted included abnormal data due to GPS measurement errors; however, more than 95% of the 1-day-long data without missing points were accepted. Therefore, it can be said that a sufficient number of features were obtained for comparison.

Figure 4 shows the plots of accepted AR and MA coefficient features that are from GPS data of five significant directions and locations to the global thermal deformation mode. In all the plots of Fig. 4a–e, it can be seen that the AR and MA coefficients are anticorrelated. Considering the points that any significant structural condition changes had not been reported during the period of GPS data acquisition, the distributions of AR and MA coefficients can be used as the compared distributions in the structural change assessment.

4 Numerical study on sensitivities of ARIMA model coefficients to structural condition changes

The AR and MA coefficients estimated from the time-series displacements at multipoint locations and directions related to the global thermal deformation mode are expected to be used as the multivariate features for the structural change monitoring. Especially in the long-span cable-stayed bridge, the changes of boundary conditions and stayed-cable tensions may affect their structural conditions significantly. A numerical study was thus conducted to verify the sensitivities of those ARIMA model coefficients to these structural changes.

4.1 Numerical data acquisition

4.1.1 FE model of a cable-stayed bridge

In the numerical study here, a FE model of a cable-stayed bridge was constructed with reference to a previous study [13], and using the Midas Civil software. The constructed FE model is shown in Fig. 5. The total bridge length was 420 m with the main span of 220 m, and the width of girder was 15.6 m. The heights of two towers were both 90 m, and the girder was supported by two planes of stayed-cables in the fan-type arrangement. The stayed-cables were placed at intervals of 10 m on the girder; thus, the length of cables was in the range of 43.04–114.66 m. The girder and towers were modeled by the beam element, and the cable element in the software was used for the stayed-cables. The properties of each structural section are summarized in Table 1. The properties of boundary conditions were given by the linear spring stiffness at the locations of two link parts between the tower and the girder, and both ends of the girder. The spring stiffness in the longitudinal and lateral directions D_x and D_y was determined to be 7×10^5 kN/m, which were properties of the assumed rubber bearing. The fixed conditions were applied in the other directions, and the boundary conditions at the bases of two towers were the fixed-end conditions. The initial tensions of stayed-cables were determined by the pre-calculation scheme in the software to apply the geometric stiffness.

4.1.2 Input air temperature and output responses

The input load to the constructed FE model was the daily periodic air temperature load to obtain the static displacements of the global thermal deformation. Here, the 1-day air temperature time-history was set as described in the following equation:

$$f(t) = A \sin\left(\frac{2\pi}{T}t\right) + B, \quad (2)$$

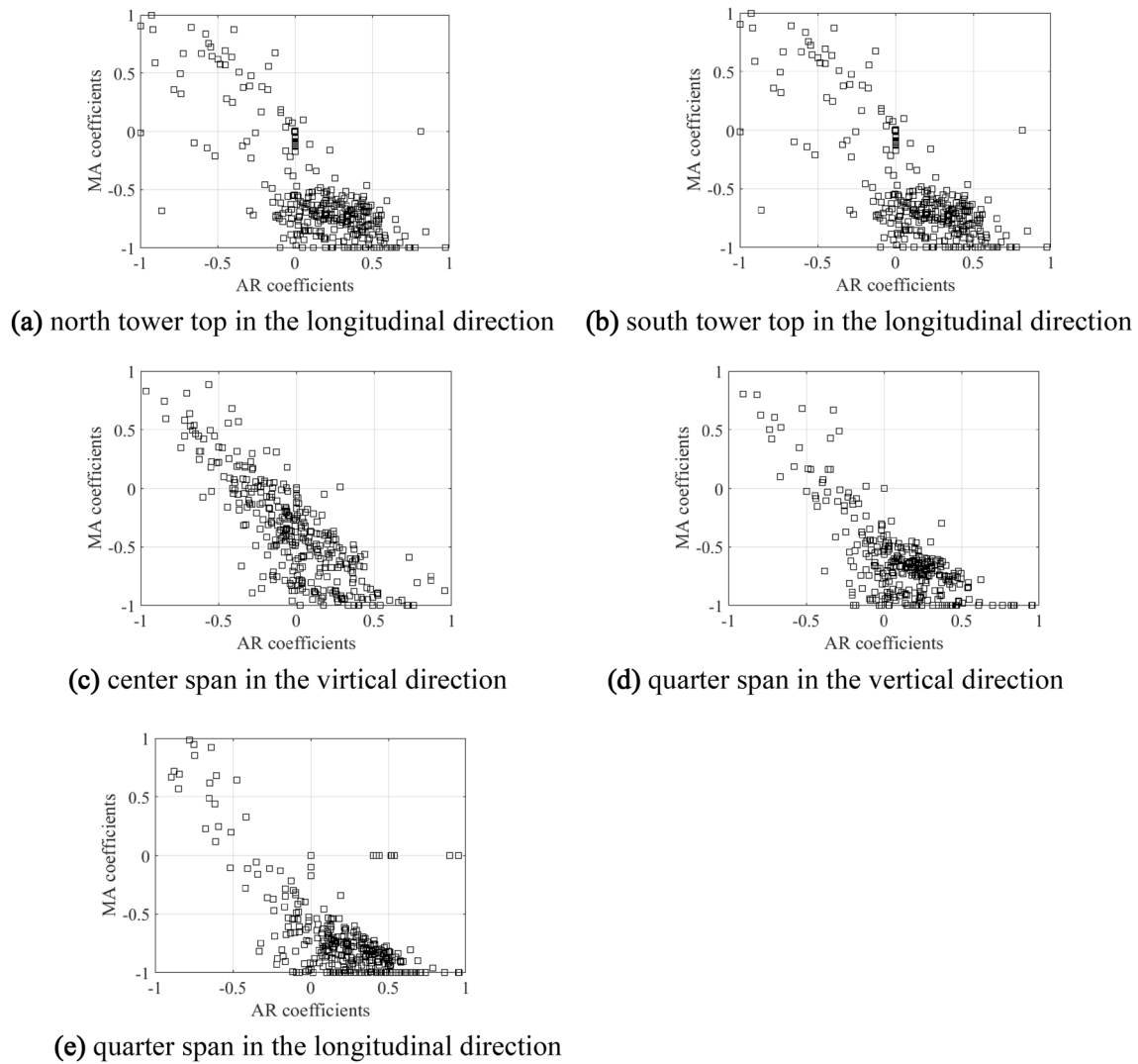
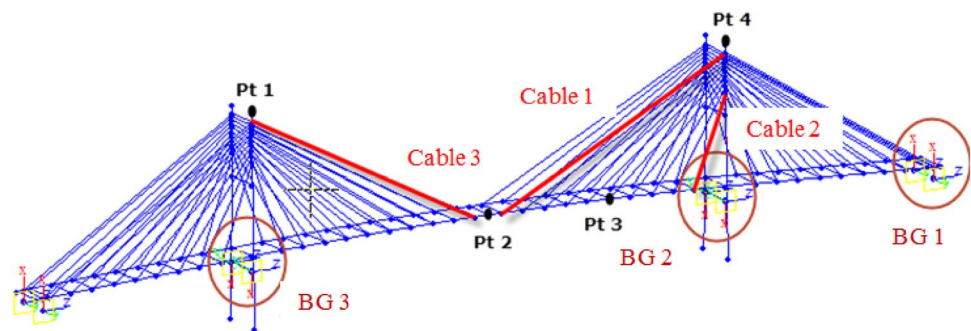


Fig. 4 Distributions of AR and MA coefficients extracted from GPS data from Jan 1 to Nov 30, 2013

Fig. 5 FE model and locations of sensing points (Pt 1–4) and structural changes (BG 1–3 and Cable 1–3)



where t was the time, T was the 1-day period of sinusoidal function, A and B were the amplitude and average of air temperature, which were set to $2\text{ }^{\circ}\text{C}$ and $27\text{ }^{\circ}\text{C}$, respectively. The time interval of temperature analysis was set to 10 min, which was the same interval as that of GPS monitoring data,

and the thermal stress analysis was conducted in each step of the temperature history. In each calculation step, the geometric nonlinearity of the stayed-cables was considered by checking convergence of stability. The length of obtained

Table 1 Properties of cable and beam elements of the cable-stayed bridge FE model

Section	Area (m ²)	Modulus of elasticity (kN/m ²)	Poisson's ratio	Density (kN/m ³)
Cable	0.0052	1.96×10^8	0.3	77.09
Girder	0.31	2.00×10^8	0.3	77.09
Pylon of tower	9.2	2.78×10^7	0.2	23.56
Cross beam of girder	0.05	2.00×10^8	0.3	77.09
Cross beam of tower	7.2	2.78×10^7	0.2	23.56

time-history was 3024 points, which was equal to 21 days with 10-min interval.

The 1-day-long time-series of displacement was then obtained at each of the five locations and directions, which were significant to the global thermal deformation mode: in the longitudinal directions at the tops of two towers, in the vertical direction at the mid-span, in the vertical and longitudinal directions at the quarter span, and the locations of which are indicated as Pt #1–#4 in Fig. 5. To use them as the data in ARIMA model estimation, the random white noise was added to each time-series. Here, the noise level was determined by the GPS specifications: 25% noise to the amplitude of periodic response in the longitudinal and lateral directions (x - and y -directions), and 12% noise in the vertical

direction (z -direction). Figure 6 shows one of numerical time-series data with random noise in the nominal structural condition according to the five significant directions.

4.1.3 Structural changes

The feature of ARIMA model coefficients that applied to the global thermal deformation was expected to show sensitivities to the global structural changes: here, the changes of bridge boundary conditions and the changes of stayed-cable tensions. The cases of those structural changes for the verification were then set up as shown in Table 2. In the cases of boundary condition changes, BC #1–#3, the spring stiffness D_x and R_y were increased to simulate the hardening of

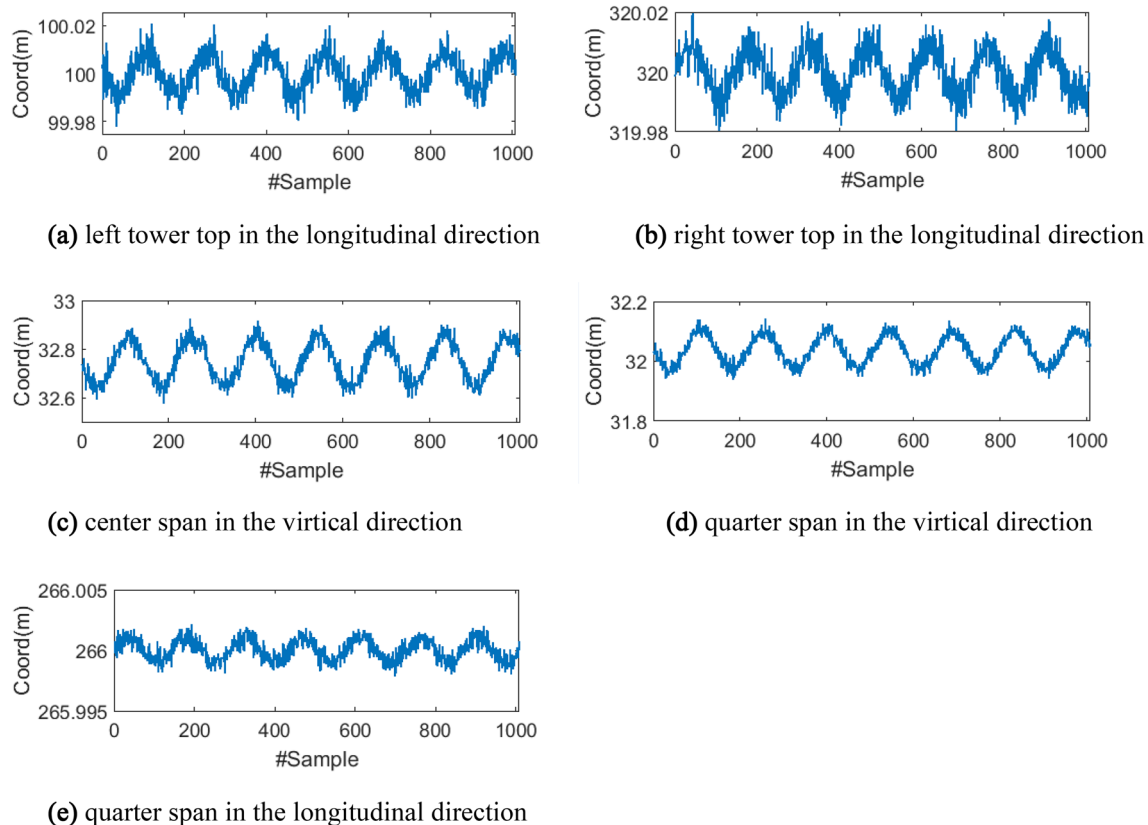


Fig. 6 Numerical time-series data under the periodic air temperature time-history (7-days long) in the nominal structural condition

Table 2 Case of structural changes

Case #	Location	Structural changes
Nominal	–	–
BC #1	BG1	$D_x\text{-H}^a$
BC #2 (-H/-VH)	BG2	$D_x\text{-H}^a$ $D_x\text{-VH}^b$
BC #3	BG3	$D_x\text{-H}^a$
TC #1 (-5/-10/-25/-50)	Cable 1	5% tension reduction 10% tension reduction 25% tension reduction 50% tension reduction
TC#2	Cable 2	10% tension reduction
TC#3	Cable 3	10% tension reduction

^aHigh stiffness: $D_x\text{-H} = D_x (\text{nominal}) \times 10^4$

^bVery high stiffness: $D_x\text{-VH} = D_x \times 10^{20}$ (near fixed condition)

rubber bearings due to the deterioration. The effect of location was verified by comparing the cases of BC #1–3 with “-H”, and that of the degree of hardening was examined by comparing between “-H” and “-VH” in BC #2. Notice that the spring stiffness in “-VH” was set as sufficiently large values so that the displacement outputs showed almost the same outputs in the case of fixed conditions. In the case of tension changes, TC #1–#3, the tension of a stayed-cable was reduced at each of three locations, indicated in Cable 1–3 in Fig. 5. In addition, the effect of degree of tension reduction was also investigated in the case of TC #2. In each case, the numerical data, which were the displacement under the periodic thermal load history with random noise, were obtained at the five locations, which were significant to the global thermal deformation mode.

4.2 Comparison of AR and MA model coefficients in varying structural conditions

The ARIMA model coefficients were then extracted from the numerical time-series data under each of structural

conditions by following the procedure of Step 1–5 explained in Sect. 3.1. Here, the orders of ARIMA model were determined to ARIMA (1,1,1) in Step 1–3. Figure 7 shows one of results of ARIMA model estimation in Step 4. Here, it can be seen that the estimated ARIMA model in red line well overlays the original 1-day-long time-series displacement in blue line in Fig. 7a, and the standardized residual errors follow the normal distribution as shown in Fig. 7b, c. This can indicate that the residual errors are the samples of the white noise process. In the Ljung–Box test in Step 5, the null hypothesis, the residual error process did not show the autocorrelation, were not rejected with p values of [0.15, 0.28, 0.08] at lags [3, 6, 9], higher than 0.05. It could then be concluded that the ARIMA model was estimated properly, and the AR and MA coefficients could be accepted as the features. In each case of structural condition, the number of 1-day-long data was 21, and most of them, 20 out of 21 in most cases, could give the accepted AR and MA coefficient features.

Figures 8 and 9 show the comparisons of the AR and MA coefficient distributions in the cases of boundary condition changes and the stayed-cable tension changes, respectively. In the case BC#2 with increasing the spring stiffnesses at BC-2, all distributions of the AR and MA coefficients show the negative regressions as shown in Fig. 8a–e. The distributions from the data at two tower tops in the longitudinal direction, which are shown in Fig. 8a, b, almost overlapped even in the different degree of boundary condition changes. On the other hand, in the results of the center and quarter spans in the vertical direction, which are shown in Fig. 8c, d, the AR and MA coefficients in the case of BC#2-VH are distributed in the higher range of MA value compared to the distributions in the cases of nominal and BC#2-H. Also in Fig. 8e, which is from the data at the quarter span in the longitudinal direction, the distribution in the case of BC#2-H seems to show the different regression from those in the case of nominal condition and BC#2-VH. In TC#1, which is the case of tension reduction on Cable-1, shown in Fig. 9, there

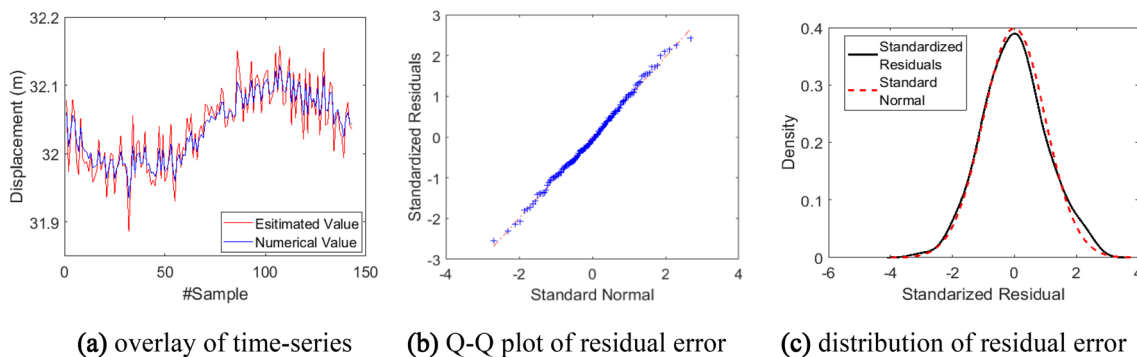


Fig. 7 Estimated ARIMA model to one of 1-day time-series displacement

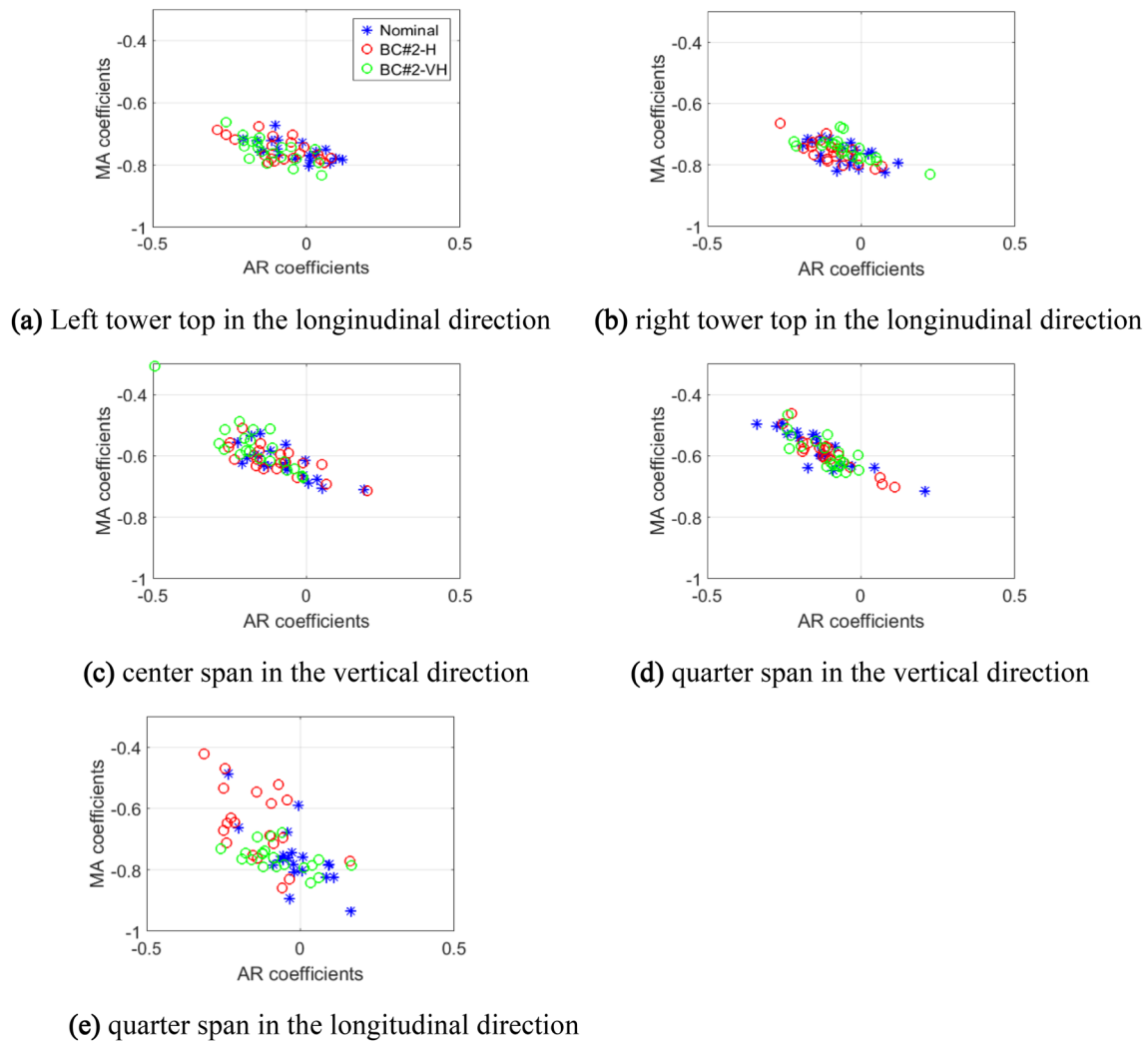


Fig. 8 AR and MA coefficients' comparison in the different degrees of increasing spring stiffness at BC-2

is the negative regression in the plots for all sensor positions, however, changes in the AR and MA coefficient distributions are not clearly recognized. In conclusion here, there seems to be some changes in the AR and MA coefficient distribution in each case of structural changes. However, it is difficult to evaluate those changes directly from the distributions of coefficients. This was why the multivariate comparison of the AR and MA coefficients was required.

5 Structural change monitoring by ARIMA model coefficient comparison

The Mahalanobis distance was adapted to compare the feature vector of multivariate AR–MA coefficients extracted from time-series displacement data at the significant locations and directions of the global thermal deformation. Here, the sensitivities of Mahalanobis distance measures in the

changes of boundary conditions and stayed-cable tensions are first verified in the numerical study. And then, the application to GPS monitoring data acquired in the actual cable-stayed bridge is presented for discussing the effectiveness of using the ARIMA model coefficients as the comparative feature to the structural change monitoring.

5.1 Procedure of Mahalanobis distance comparison

The Mahalanobis distance (MD) is the statistical distance of multivariate vectors, each of whose components is the random variable. While the feature comparison based on the MD has been adopted in many SHM studies, in this study, the procedure of comparison between a MD distribution of the baseline data and that of the compared data [14] was adopted to evaluate the structural changes. Here, the baseline dataset, which is the time-series data under the structural condition without any significant changes, is first configured, and the feature

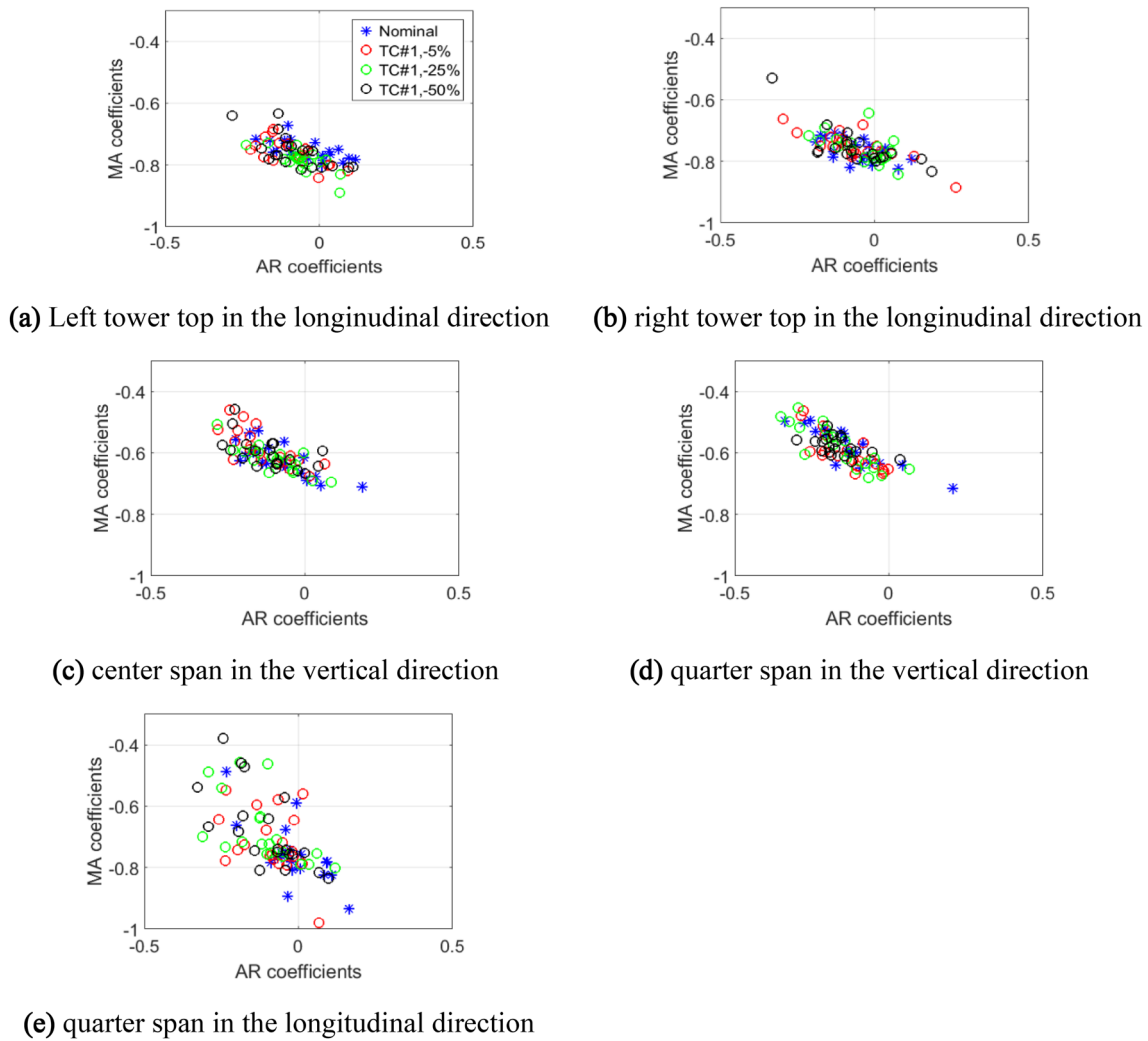


Fig. 9 AR and MA coefficients' comparison in the different degrees of stayed-cable tension changes

vectors of this baseline dataset are extracted by applying the procedure of Step 1–5 presented in Sect. 3.1. The Mahalanobis distance of i -th 1-day-long time-series data, MD_i^B , is calculated as below:

$$MD_i^B = \sqrt{(\mathbf{x}_i^B - \bar{\mathbf{x}}_B)^T \mathbf{S}_B^{-1} (\mathbf{x}_i^B - \bar{\mathbf{x}}_B)}, \tag{3}$$

where \mathbf{x}_i^B is the feature vector extracted from i -th baseline 1-day-long data, and $\bar{\mathbf{x}}_B$ and \mathbf{S}_B are the mean vector and the covariance matrix of the feature vectors derived from the baseline dataset. When the compared time-series data are acquired, their feature vectors are obtained by applying the same process, Step 1–5, and the Mahalanobis distance of j -th compared 1-day-long time-series data, MD_j^C , can then be calculated by the following formula:

$$MD_j^C = \sqrt{(\mathbf{x}_j^C - \bar{\mathbf{x}}_B)^T \mathbf{S}_B^{-1} (\mathbf{x}_j^C - \bar{\mathbf{x}}_B)}. \tag{4}$$

This is the statistical distance from the distribution of the baseline feature vector sets.

5.2 Mahalanobis distance comparison in the structural changes

In the numerical study to verify sensitivities of the Mahalanobis distance (MD) to the structural changes of boundary conditions and the stayed-cable tensions, the baseline data for MD^B were the time-series displacement under the nominal structural conditions. The number of feature vectors was 20; i.e., $i = 1-20$ in Eq. (3), that was the number of 1-day-long time-series data accepted in Step 5 of the feature extraction procedure.

5.2.1 Boundary condition changes

Figure 10a, b shows the results of Mahalanobis distance comparisons in the case of different locations of boundary condition (BC) changes, and in the case of the spring stiffness increase, respectively. The green-dotted line indicated in each of both figures is the reference line, which indicates $\mu + \sigma$, where μ and σ are mean and standard deviation of MD_i^B ($i = 1-20$), respectively. In both figures, the Mahalanobis distances of compared data MD^C are distributed in higher MD values compared to the distribution of MD^B . However, it is difficult to recognize the degree of BC changes because the distributions of two cases, BC#2-H and BC#2-VH, do not show significant difference in Fig. 10a. On the other hand, it was considered that the relative location of BC change to the sensor locations has sensitivity to the MD distribution. It can be seen that the fluctuation range of MD^C in the case of BC#3 is larger than those in the cases of BC#1 and BC#2 in Fig. 10b. It was considered that the data from the sensor at the quarter span gave the sensitivity to the location of BC change. From the results here, it can be said that the detection of BC change is possible by the MD comparison of the ARIMA model coefficient feature vector. The relationship between the locations of BC changes and sensor locations is worth being considered by evaluating the effect of BC changes to the global thermal deformation.

5.2.2 Stayed-cable tension changes

Figure 11a shows the MD comparison within the cases of four degrees of tension reductions at the same stayed-cable, Cable-1. The baseline data and the reference line are the same ones as those in Fig. 10. First, it can be clearly seen that the MD^C in all of four cases are distributed in higher MD value ranges than the baseline distribution. The feature

of ARIMA model coefficients is applicable to the detection of stayed-cable tension changes. Moreover, as the degree of tension reduction increases, the number of samples that exceeds the reference line increases, i.e., 85% in the case of -5% reduction, 80% in the case of -10% reduction, 75% in the case of -25% reduction, and 90% of samples exceed the reference line in the case of -50% tension reduction. Moreover, the fluctuation range of MD^C distribution also increases because the maximum MD^C increases as the stayed-cable tension is reduced. It was expected that the feature vector of ARIMA model coefficients has the sensitivities to the degree of tension reduction at the stayed-cable. On the other hand, it is difficult to find the sensitivities to the location of tension reduction, as shown in Fig. 11b, even though the Mahalanobis distance distributions in the cases of TC#1-#3 also indicate the occurrence of tension reduction.

5.3 Application to the GPS monitoring data

The Mahalanobis distance comparison was then applied to the feature vector of AR and MA coefficients extracted from the year-round GPS monitoring data acquired in the cable-stayed bridge, which are shown in Sect. 3.2. Here, the baseline data for MD^B were configured by the first 6 months of the time-series data, from Jan 1 to June 30, 2013, and the compared data MD^C were the later 5 months of the data, from July 1 to Nov 30, 2013. In the result of MD comparison, which is shown in Fig. 12, the baseline MDs in black line and compared MDs in red-dotted line are distributed in the same range of MD value. Notice that any significant structural changes were not recognized in the inspection conducted by the bridge owner during the period of those data acquisition in 2013. The result here can present the applicability of feature vector of the ARIMA model coefficients and the Mahalanobis distance comparison to the

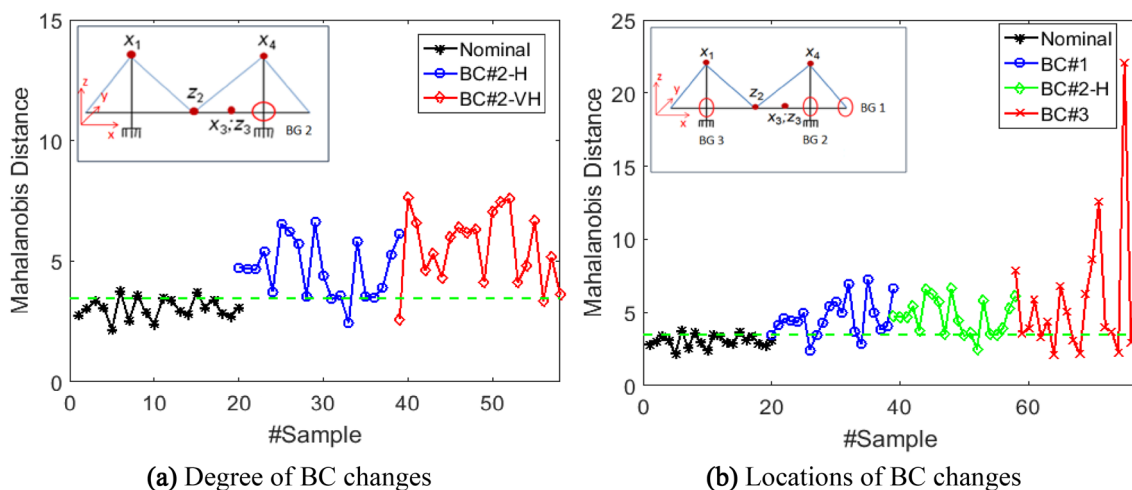


Fig. 10 Mahalanobis distance comparison in the boundary condition (BC) changes

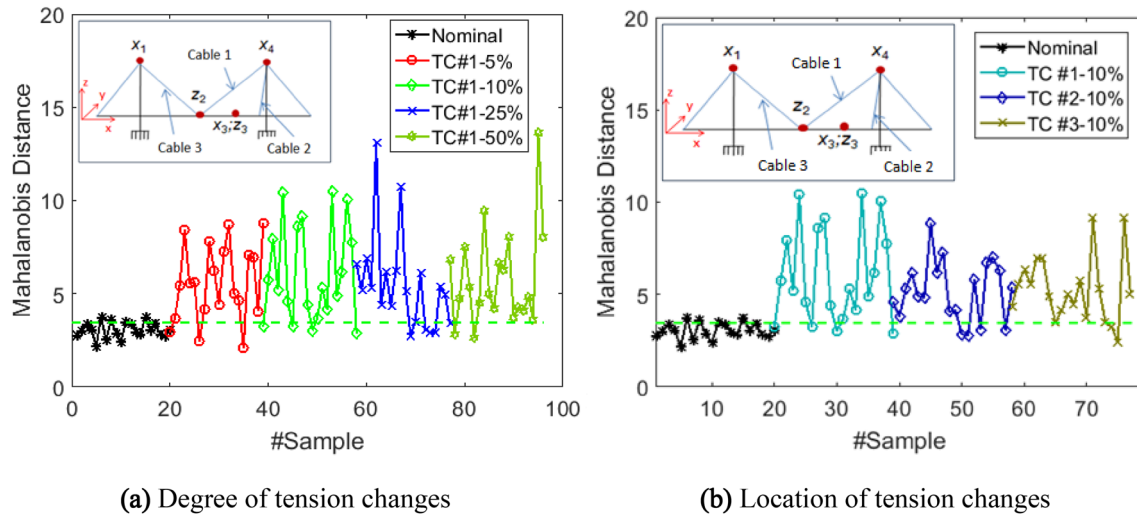


Fig. 11 Mahalanobis distance comparison in the stayed-cable tension changes

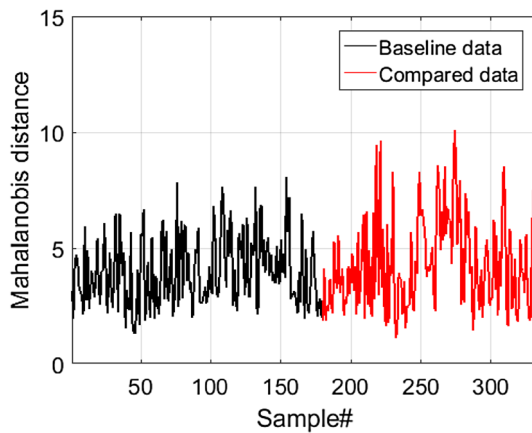


Fig. 12 Mahalanobis distance comparison of GPS monitoring data with baseline data from Jan 1st to June 30th, and compared data from July 1st to Nov 30th, 2013

structural change monitoring using long-term GPS monitoring data in terms of the global thermal deformation.

6 Conclusions

In this paper, the use of ARIMA model coefficients extracted from the time-series response of the global thermal deformation mode, which can be acquired by the GPS monitoring, was proposed for the structural change monitoring in the long-span bridge. The feature extraction and comparison procedures were presented, and its applicability was verified both by the numerical study and the application to actual GPS monitoring data. In the numerical study using a FE model of a cable-stayed bridge, it was shown that the changes of boundary conditions and stayed-cable tensions

could be clearly detected in the Mahalanobis distance comparison of the feature vector, which was configured by the estimated AR and MA coefficients from the time-series displacement of significant locations and directions to the global thermal deformation. The procedure was then applied to year-round GPS data acquired in an actual cable-stayed bridge. It was then shown that the Mahalanobis distance comparison could provide proper assessment to the structural changes that was consistent with the actual structural condition. The sensitivities to recognize detailed locations and degrees of those structural changes should be further investigated. However, the effectiveness of using the global thermal deformation, which was the response to the air temperature load, in SHM could be shown in this study. The effects of daily temperature changes are included in most SHM data acquired in civil structures. The feature extraction and comparison procedure proposed in this study can be expected to be applied to time-series data not only from GPS but also from other sensors if it is greatly affected by the daily temperature change.

References

1. Cross EJ, Koo KY, Brownjohn JMW, Worden K (2010) Long-term monitoring and data analysis of the Tamar bridge. *Mech Syst Signal Process* 35(1–2):16–34
2. Zhou Y, Sun L, Peng Z (2015) Mechanisms of thermally induced deflection of a long-span cable-stayed bridge. *Smart Struct Syst* 15(3):505–522
3. Rolands K, Prakash K, Bill H (2015) Long-term structural health monitoring of the Cleddau bridge: evaluation of quasi-static temperature effects on bearing movements. *Struct Infrastruct Eng* 12(10):1342–1355
4. Fujino Y, Murata M, Okano S, Takeguchi M (2000) Monitoring system of the Akashi Kaikyo Bridge and displacement

- measurement using GPS. In: *Nondestructive Evaluation of Highways, Utilities, and Pipelines IV*, 3995. International Society for Optics and Photonics, pp 229–237
5. Celebi M (2000) GPS in dynamic monitoring of long-period structures. *Soil Dyn Earthq Eng* 20(5–8):477–483
 6. Kaloop MR, Li H (2009) Monitoring of bridge deformation using GPS technique. *KSCE J Civ Eng* 13(6):423–431
 7. Le VH, Nishio M (2015) Time-series analysis of GPS monitoring data from a long-span bridge considering the global deformation due to air temperature changes. *J Civ Struct Health Monitor* 5(4):415–425
 8. Sohn H, Farrar CR (2001) Damage diagnosis using time series analysis of vibration signals. *Smart Mater Struct* 10(3):446–451
 9. Kaloop MR, Hussan M, Kim D (2019) Time-series analysis of GPS measurements for long-span bridge movements using wavelet and model prediction techniques. *Adv Space Res*. <https://doi.org/10.1016/j.asr.2019.02.027>
 10. Omenzetter P, Brownjohn JMW (2006) Application of time series analysis for bridge monitoring. *Smart Mater Struct* 15(1):129–138
 11. Shi H, Worden K, Cross EJ (2019) A cointegration approach for heteroscedastic data based on a time series decomposition: an application to structural health monitoring. *Mech Syst Signal Process* 120:16–31
 12. Hamilton JD (1994) *Time series analysis*. Princeton University Press, Princeton
 13. Vikas AC, Prashanth MH, Indrani G, Channappa TM (2013) Effect of cable degradation on dynamic behavior of cable stayed bridges. *J Civ Eng Res* 3(1):35–45
 14. Worden K, Manson G, Fieller NR (2000) Damage detection using outlier analysis. *J Sound Vib* 229(3):647–667

Publisher's Note Springer Nature remains neutral with regard to jurisdictional claims in published maps and institutional affiliations.